Noncovalent Functionalization of Graphene Attaching [6,6]-Phenyl-C61-butyric Acid Methyl Ester (PCBM) and Application as Electron Extraction Layer of Polymer Solar Cells

Shuxuan Qu, Minghua Li,[†] Lixin Xie, Xiao Huang, Jinguo Yang, Nan Wang, and Shangfeng Yang*

Hefei National Laboratory for Physical Sciences at Microscale, CAS Key Laboratory of Materials for Energy Conversion & Department of Materials Science and Engineering, University of Science and Technology of China (USTC), Hefei 230026, China. [†]Present address: Department of Chemistry and Materials Engineering, Hefei University, Hefei 230601, China.

ABSTRACT A new graphene—fullerene composite (rGO-pyrene-PCBM), in which [6,6]-phenyl-C61-butyric acid methyl ester (PCBM) was attached onto reduced graphene oxide (rGO) *via* the noncovalent functionalization approach, was reported. The pyrene-PCBM moiety was synthesized *via* a facile esterification reaction, and pyrene was used as an anchoring bridge to link rGO and PCBM components. FTIR, UV—vis, and XPS spectroscopic characterizations were carried out to confirm the hybrid structure of rGO-pyrene-PCBM, and the composite formation is found to improve greatly the dispersity of rGO in DMF. The geometric configuration of rGO-pyrene-PCBM was studied by Raman, SEM, and AFM analyses, suggesting that the C_{60} moiety is far from the graphene sheet and is bridged with the graphene sheet *via* the pyrene anchor. Finally rGO-pyrene-PCBM was successfully applied as electron extraction layer for P3HT:PCBM bulk heterojunction polymer solar cell (BHJ-PSC) devices, affording a PCE of 3.89%, which is enhanced by *ca.* 15% compared to that of the reference device without electron extraction layer (3.39%). Contrarily, the comparative devices incorporating the rGO or pyrene-PCBM component as electron extraction layer showed dramatically decreased PCE, indicating the importance of composite formation between rGO and pyrene-PCBM components for its electron extraction property.

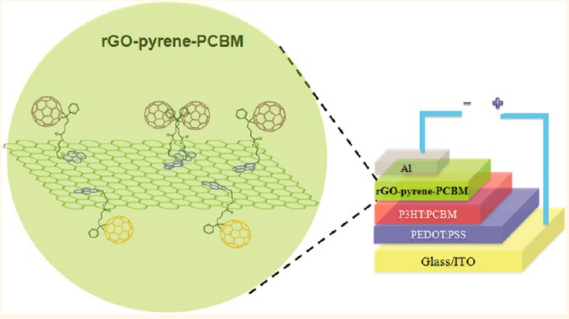

KEYWORDS: graphene · [6,6]-phenyl-C61-butyric acid methyl ester (PCBM) · pyrene · electron extraction layer · polymer solar cells

Graphene as an allotrope of carbon constituted with two-dimensional sp^2-hybridized carbon atoms has been attracting considerable attention since its discovery in 2004 by Geim and co-workers.[1] The exceptional electronic, optical, mechanical and thermal properties of graphene, featured by the high carrier mobility at room temperature (~15 000 $cm^2 V^{-1} s^{-1}$),[2] unusual quantum Hall effect,[3] good optical transparency (~97.7%),[4] large theoretical specific surface area (2630 $m^2 g^{-1}$),[5] high Young's modulus (~1 TPa),[6] and excellent thermal conductivity (3000—5000 W $m^{-1} K^{-1}$),[7] have promised its versatile potential applications in, *e.g.*, organic solar cells,[8,9] field-effect transistors,[10] and supercapacitors.[5] In specific, the applications of pristine and functionalized graphenes in bulk heterojunction polymer solar cells (BHJ-PSCs) have been extensively reported in recent years, for which graphenes were applied with different functions.[8,11—18] Because of the excellent conductivity, good flexibility, and transparency, graphenes were primarily used as transparent electrode materials aiming to replace the commonly used indium tin oxide (ITO) electrode which suffers from several problems such as high cost, the limited source of indium on earth *etc.*[13—15] Alternatively, in a few reports, functionalized graphenes have been used as electron acceptor materials in active layer due to its higher electron mobility than fullerene derivatives, large surface area for donor/acceptor interfaces and continuous pathway for the electron transfer as a result of the two-dimensional

* Address correspondence to sfyang@ustc.edu.cn.

Received for review January 14, 2013 and accepted April 15, 2013.

Published online April 15, 2013
10.1021/nn4001963

structure.[17] Furthermore, graphene oxide (GO) was also demonstrated to function as an interface layer material for hole transport in order to replace the commonly used poly(3,4-ethylendedioxythiophene): poly(styrenesulfonate) (PEDOT:PSS) which is acidic and, owing to its hygroscopicity, might damage the ITO electrode.[16] Note that, for the latter application, GO and reduced graphene oxide (rGO) generally acted as hole transport layer, while up to now, the application of GO or rGO as electron extraction layer, which is as important as the hole transport layer in BHJ-PSCs,[8] has been rarely reported. To the best of our knowledge, only recently Dai *et al.* successfully enabled a functionalized graphene as an excellent electron extraction layer, which was a cesium-neutralized graphene oxide (GO-Cs) synthesized from the simple charge neutralization of the periphery −COOH groups of GO with Cs_2CO_3. Interestingly, in both normal and inverted BHJ-PSC devices, GO-Cs and the pristine GO acted as the excellent electron extraction and hole transport layer, respectively; accordingly, an ambipolar transporting property of graphene was demonstrated.[18] Therefore, the application of functionalized graphene as an electron extraction layer of BHJ-PSCs appears quite challenging yet.

To harness the fascinating properties of graphene toward versatile applications, it is desirable to incorporate graphene with other functional materials in composite forms rather than the random mixtures.[8,13,19−25] So far a wealth of graphene-based composites have been constructed *via* both covalent and noncovalent functionalization approaches, which are based on compositions of graphene with polymers,[21] inorganic nanostructures,[22] large aromatic molecules,[23] carbon nanotubes (CNTs),[24] fullerenes,[25−28] *etc*. In particular, graphene−fullerene composites as the hybrid architectures of two allotropes of carbon with two- and zero-dimensions, respectively, have been constructed in few reports, which may combine the strong electron-accepting ability of fullerene and excellent charge transport property of graphene and hold great potential in the conceptually new all-carbon solar cells.[24−30] Chen *et al.* synthesized two types of graphene−fullerene composites *via* the covalent functionalizations of GO with pyrrolidine fullerene or fullerenol, for which the latter one exhibited enhanced nonlinear optical performance compared to the individual components.[27,31] Note that, in these studies, fullerenes were grafted only on the edge of graphene and thus the attached fullerenes may not be able to facilitate the exfoliation of graphene sheets. Wang *et al.* synthesized a new graphene−fullerene composite in which fullerene was intercalated with GO *via* the Fisher esterification between the hydroxyl groups in graphite oxide and the carboxyl groups in fullerenoacetic acid; in this way, fullerene moieties were grafted on both sides of graphene and helped to exfoliate graphene sheets.[26] More recently, Dai *et al.* synthesized C_{60}-grafted graphene nanosheets by covalently attaching monosubstituted C_{60} onto graphene sheets *via* a lithiation reaction, which was applied as the electron acceptor material in poly(3-hexylthiophene-2,5-diyl) (P3HT)-based BHJ-PSCs. The C_{60}-grafted graphene:P3HT device exhibited the best power conversion efficiency (PCE) of 1.22%, which is much higher than those of C_{60}/graphene mixture:P3HT and C_{60}:P3HT devices.[32] Despite such success on synthesizing different graphene−fullerene composites *via* covalent functionalization approach, so far there has been few reports on noncovalent functionalization of graphene by fullerene, which is however beneficial to maintain the integrity of sp^2-hybridized carbon network and consequently the outstanding conductivity of graphene.

In this paper, we report the preparation of a new graphene−fullerene composite in which [6,6]-phenyl-C61-butyric acid methyl ester (PCBM) as the most commonly used acceptor material in the state-of-art BHJ-PSCs was attached onto rGO *via* the noncovalent functionalization approach for the first time. Pyrene was used as the anchoring group for linking PCBM and rGO components, and the attached PCBM moiety is beneficial for prohibiting the restacking of graphene sheets. The as-synthesized graphene−fullerene composite was applied in P3HT:PCBM BHJ-PSC devices as electron extraction layer, and its effect on the device performance of P3HT:PCBM BHJ-PSCs is investigated in detail.

RESULTS AND DISCUSSION

Synthesis and Characterization of rGO-Pyrene-PCBM. The synthesis route of **rGO-pyrene-PCBM** is illustrated in Scheme 1. As the first step, the pendant **pyrene-PCBM** was synthesized *via* the facile esterification reaction of PCBA (step (i)), which was obtained from the acidification of PCBM.[33−35] The chemical structure of **pyrene-PCBM** was determined by ^{1}H NMR spectroscopic analysis (see Supporting Information Figure S1), the appearance of strong signals of pyrene moiety confirms the successful integration of pyrene onto PCBM *via* the esterification reaction, which has been demonstrated to be one of the most efficient methods for the ester formation with high conversion rate owing to the catalytic ability of DMAP.[36]

The pyrene moiety has been demonstrated in numerous reports to have strong affinity with the basal plane of graphite *via* $\pi-\pi$ stacking as shown in versatile noncovalent composites of graphene−pyrene, and carbon nanotube (CNT)−graphene;[23,37,38] thus, pyrene was chosen as the anchoring group for linking PCBM and rGO components in our present work. The synthesis of **rGO-pyrene-PCBM** was accomplished by simply introducing **pyrene-PCBM** during the preparation of rGO[39,40] *via* the reduction of GO (Scheme 1, step (ii)), and the resultant products were characterized by several spectroscopic methods so as to ascertain its hybrid nature. Shown in Figure 1 is the FTIR spectrum of **rGO-pyrene-PCBM** (curve a) in comparison with those of GO, rGO, and

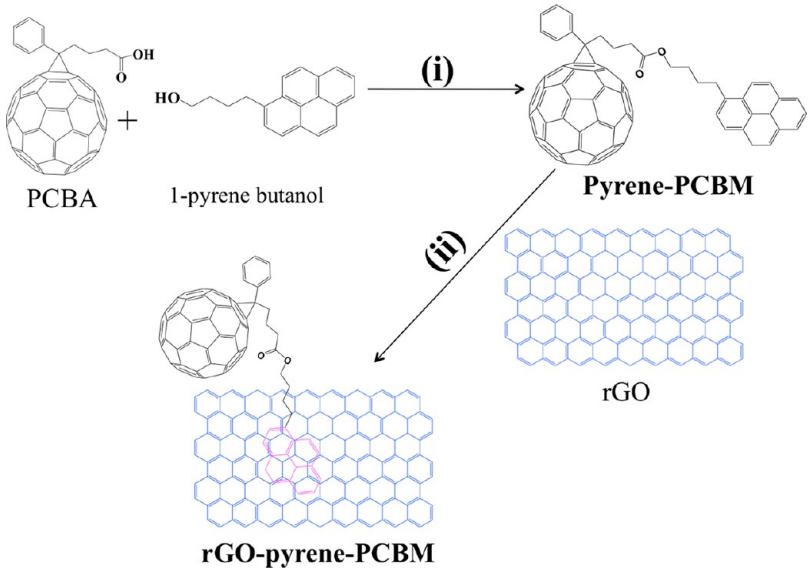

Scheme 1. Synthetic routes of rGO-pyrene-PCBM. (i) DCC and DMAP, CS_2:CH_2Cl_2 (1:1 v/v); rt.; (ii) hydrazine and ammonia, DMF; 95 °C

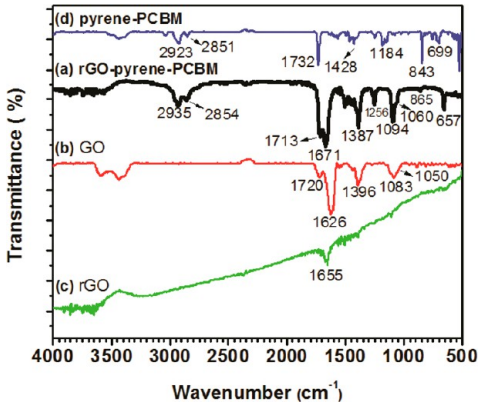

Figure 1. FTIR spectra of rGO-pyrene-PCBM (a), GO (b), rGO (c), and pyrene-PCBM (d).

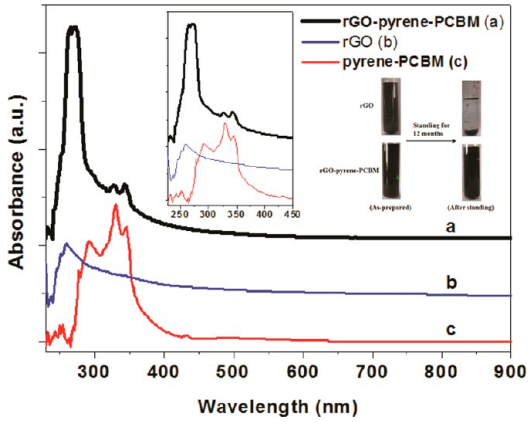

Figure 2. UV−vis spectra of rGO-pyrene-PCBM (a), rGO (b), and pyrene-PCBM (c). The insets show the enlarged spectral range of 230−450 nm and the pictures of rGO and rGO-pyrene-PCBM dispersions in DMF before and after standing for 12 months.

pyrene-PCBM components (curves b−d). Clearly, the vibrational bands correlated with the oxidation groups of GO raised from the epoxy (1050 cm^{-1}), hydroxyl (C−OH, 1083 and 1396 cm^{-1}), and carboxyl (1720 cm^{-1}) groups[26,27,41,42] became much weaker or even disappeared in rGO, while the vibrational peak at 1626 cm^{-1} assigned to the skeletal vibration of graphitic domains of GO largely remained in the FTIR spectrum of rGO. These results indicate the successful reduction of GO, which is confirmed further by AFM study below. In the FTIR spectrum of **rGO-pyrene-PCBM**, the characteristic vibrational band of rGO (1655 cm^{-1}) correlated with the skeletal vibration of graphite domains is clearly observed with a slight shift. Interestingly those vibrational bands correlated with the oxidation groups of GO are also observed in the spectrum of **rGO-pyrene-PCBM** with some shifts, suggesting that the extent of reduction of GO for **rGO-pyrene-PCBM** is lower than that for the unmodified rGO. This indicates the influence of **pyrene-PCBM** on the reduction of GO by hydrazine. On the other hand, the characteristic vibrational bands at 2851 and 2923 cm^{-1} of **pyrene-PCBM**, which correspond to the symmetric and asymmetric stretching vibrations of the alky groups, respectively, are obviously presented in the spectrum of **rGO-pyrene-PCBM** as well, confirming the existence of the **pyrene-PCBM** component within **rGO-pyrene-PCBM**. However, whether the two components of rGO and **pyrene-PCBM** exist in the form of physical mixture or composite cannot be deduced from FTIR characterization; thus, further spectroscopic characterization is needed.

Figure 2 presents the UV−vis spectra of **rGO-pyrene-PCBM**, rGO and **pyrene-PCBM**. Evidently, the two intense absorption peaks with absorption maxima at 332 and 346 nm as the characteristic absorption peaks of **pyrene-PCBM** are observed in the spectrum of **rGO-pyrene-PCBM** with slight blue-shifts (2−3 nm). Likewise,

the characteristic absorption peak of rGO at 261 nm is preserved in the spectrum of **rGO-pyrene-PCBM** as well, which experiences however an obvious red-shift and exhibits a doublet absorption feature with two maxima at 267 and 273 nm. The energy shifts of the characteristic absorption peaks of both rGO and **pyrene-PCBM** confirm that these two components exist in the composite form, otherwise a simple superposition of the absorption features of both components would be expected for their physical mixture. Considering that the pyrene and C_{60} moieties within **pyrene-PCBM** are both aromatic systems rich of π electrons, the shifts of the characteristic absorption peaks of rGO and **pyrene-PCBM** can be understood as the result of the $\pi-\pi$ stacking interactions between the graphene sheet with both pyrene and C_{60} moieties of **pyrene-PCBM**. Benefited from such intramolecular $\pi-\pi$ stacking interactions between the graphene sheet and **pyrene-PCBM**, the dispersity of **rGO-pyrene-PCBM** in DMF is greatly improved compared to the pristine rGO; as a result, the original **rGO-pyrene-PCBM** dispersion in DMF was a stable black supernatant. After standing for 12 months, the stable black supernatant of **rGO-pyrene-PCBM** remained unchanged (see inset of Figure 2). To test further the stability of the **rGO-pyrene-PCBM** supernatant, a 3 min centrifugation at 9000 rpm was carried out, and only a minute quantity of black precipitate was observed while a black homogeneous supernatant was retained, indicating the good stability of **rGO-pyrene-PCBM** dispersion in DMF.

The hybrid structure of **rGO-pyrene-PCBM** was further confirmed by XPS study. Figure 3 shows the C_{1s} XPS spectrum of **rGO-pyrene-PCBM** in comparison with that of rGO, and their characteristic binding energy data were summarized in Supporting Information Table S1, which includes the assignments of C−C (sp^2 carbon), C−O (epoxy), C═O, and O−C═O groups to the signal peaks with binding energy at 284.6, 286.0, 287.6, and 289.0 eV, respectively.[43,44] According to the comparison of the relative intensity of different carbon signals, clearly the intensity of the O−C═O signal (289.0 eV) of rGO, which is correlated with the carboxyl groups on the edge of graphene sheets and cannot be completely removed by the hydrazine reductant, is obviously weakened in **rGO-pyrene-PCBM**. On the contrary, the relative intensity of C−C (284.6 eV) signal increases dramatically in **rGO-pyrene-PCBM** (see Table S1). The increase of C−C signal is understandable because sp^2 carbon is the only construction unit of C_{60} and pyrene moieties within **pyrene-PCBM**. Hence, these results confirm once more the successful attachment of **pyrene-PCBM** moiety onto rGO.

Intramolecular Interaction and Geometric Configuration, and Film Morphology of rGO-Pyrene-PCBM. Given that the intramolecular $\pi-\pi$ stacking interactions exist within **rGO-pyrene-PCBM** composite while both pyrene and C_{60} moieties are aromatic systems rich of π electrons, it is interesting to elucidate the geometric configuration of

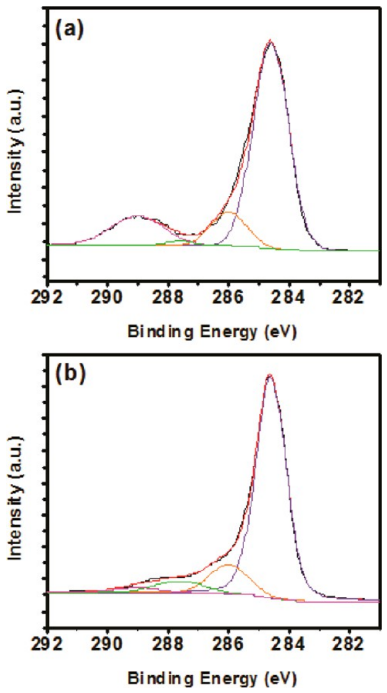

Figure 3. C_{1s} XPS spectra of rGO (a), and rGO-pyrene-PCBM (b).

rGO-pyrene-PCBM in terms of the spatial orientation of C_{60} moiety. Two different possible configurations of **rGO-pyrene-PCBM** were proposed in Scheme 2, with the discrepancy on the orientation of C_{60} moiety (attaching onto (I) or being far from (II) the graphene sheet). In both configurations, the pyrene moiety is presumed to attach onto the graphene sheet as an anchor to bridge the C_{60} moiety and graphene sheet, which is crucial for the composite formation.

Because of the sensitivity to the electronic structure of carbon nanomaterials, Raman spectroscopy provides valuable information for graphene characterization specifically the chemically functionalized graphene.[45] Figure 4 illustrates the comparison of Raman spectra of **rGO-pyrene-PCBM**, GO, rGO and **pyrene-PCBM**. There are two prominent Raman scattering peaks at 1356 and 1608 cm^{-1}, which are well-documented to correspond to D and G bands, respectively.[46,47] Clearly, the D/G intensity ratio of rGO is higher than that for GO, and this is in good agreement with the literature reports and interpreted as the result of the restoration of sp^2-hybridized carbon during the reduction reaction.[47,48] In **rGO-pyrene-PCBM** composite, both D and G bands of rGO are dramatically broadened with the superposition of the characteristic peaks from the **pyrene-PCBM** component. For the D band of **rGO-pyrene-PCBM**, the Raman scattering peaks at 1427 and 1463 cm^{-1} observed in **pyrene-PCBM** appear as the shoulder peak of the intense D band of rGO, which keeps almost unshifted compared to that of the pristine rGO. Similarly, the G band of **rGO-pyrene-PCBM** is slightly down-shifted to 1597 cm^{-1}. The down-shifting of the G band of rGO was reported in the composite comprising reduced graphene sheets (ReG, which

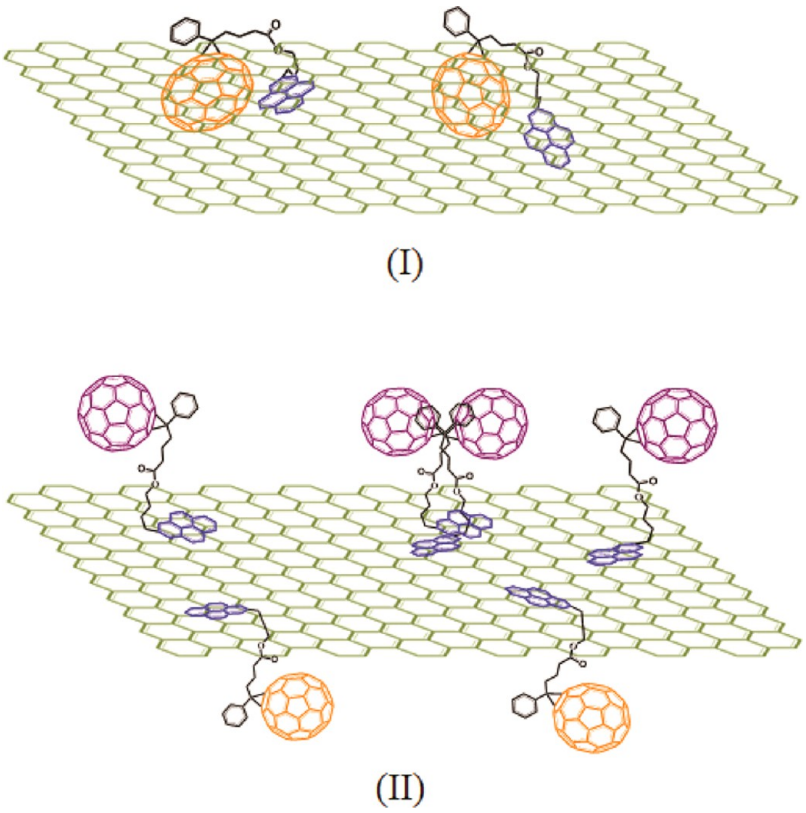

Scheme 2. Schematic illustrations of two possible conformations of rGO-pyrene-PCBM with the orientation of C_{60} moiety attaching onto (I) or being far from (II) the graphene sheet

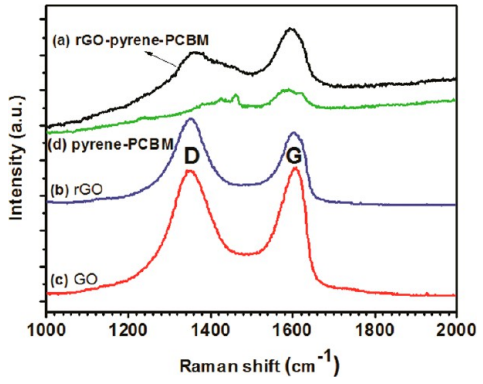

Figure 4. Raman spectra of rGO-pyrene-PCBM (a), rGO (b), GO (c), and pyrene-PCBM (d).

is same to rGO) and large aromatic molecules such as pyrene-1-sulfonic acid sodium salt (PyS), and was interpreted by the change of the concentration of carrier in the plane of graphene because of the additional charge carriers brought by dispersant aromatic molecules, leading to the Fermi level shift.[23] Interestingly, it has been also reported that the G-band of ReG was upshifted upon forming the composite with such electron acceptor as the diasodium salt of 3,4,9,10-perylenetetracarboxylic diimide bisbenzenesulfonic acid (PDI).[23] Similarly, the charge transfer between the rGO and **pyrene-PCBM** should be responsible for the downshifting of the G band of rGO with **pyrene-PCBM** acting presumably as donor for our case. Furthermore, the finding of the downshifting of the G band of rGO resulting from the attachment of the **pyrene-PCBM** moiety suggests that very likely the **pyrene-PCBM** moiety attaches to graphene sheet *via* the pyrene bridge as the donor group rather than directly attaching onto the graphene sheet (see configuration (II), Scheme 2), because otherwise the well-known strong electron-accepting ability of C_{60} would inevitably interfere with the charge transfer between **pyrene-PCBM** and graphene sheet.

The configuration of **rGO-pyrene-PCBM** proposed above was further confirmed by SEM study (Figure 5). Compared to the surface of the GO film, there seems to be no significant change on the feature of the rGO film except the decrease of the size of graphene sheets, which is due to the fragmentation brought from the reduction reaction of GO because of the removal of the oxidation groups of GO by reduction. On the other hand, in the SEM images of **rGO-pyrene-PCBM**, the flakiness of graphene sheets cannot be observed clearly; instead a continuous film with lots of interconnected spherical particles was found, which is presumably attributed to the aggregation of the C_{60} moieties. Thus, such an aggregation feature confirms that the C_{60} moieties within **pyrene-PCBM** are far from the graphene sheet, otherwise, their direct attachments onto the graphene sheets would prohibit their aggregations. Noteworthy, the continuous film structure accessible by **rGO-pyrene-PCBM** reveals that **pyrene-PCBM**

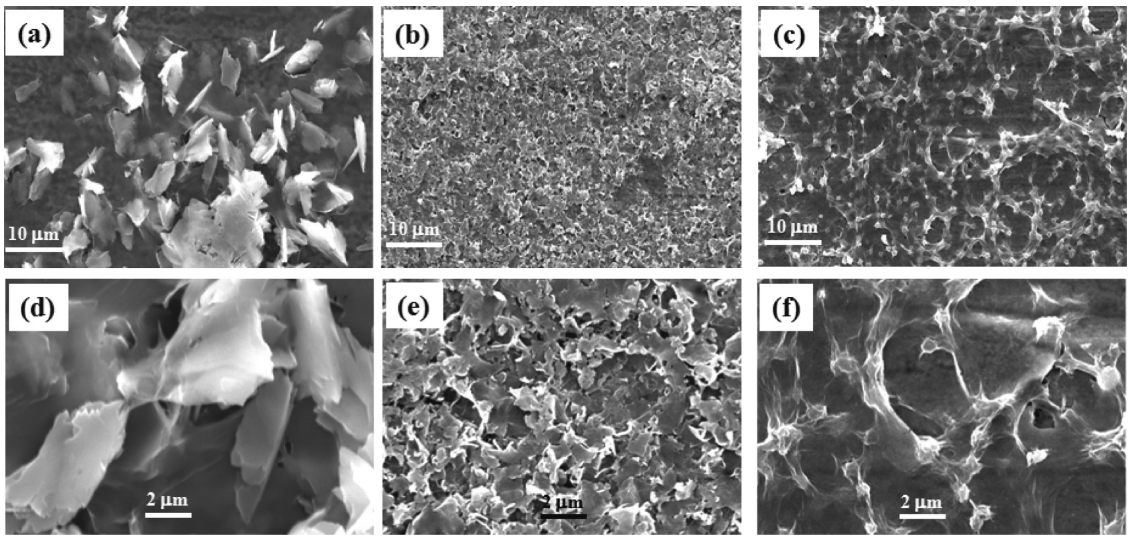

Figure 5. SEM images of GO (a and d), rGO (b and e) and rGO-pyrene-PCBM (c and f) with different length scales.

improves the film formation ability of graphene sheets, which endues the potential application of **rGO-pyrene-PCBM** composite in, *e.g.*, polymer solar cells as described in details below.

The film morphologies of GO, rGO, and **rGO-pyrene-PCBM** were then measured by AFM so as to determine their thickness, for which the films were prepared by depositing the corresponding dispersions in DMF on fresh cleaved mica and dried in atmosphere at room temperature. Figure 6a,d shows that the thickness of GO was ~0.9 nm, which is comparable to that reported in the literature and suggests that the GO we prepared is a single-layer graphene sheet.[23,49] Upon the reduction from GO to rGO, the thickness of rGO decreases slightly to 0.6−0.8 nm as observed in Figure 6b,e. This indicates the removal of the oxidation groups of GO and confirms once more the successful reduction of GO. Interestingly, after the attachment of **pyrene-PCBM** moiety, the thickness of **rGO-pyrene-PCBM** composite increases dramatically up to ~3.0 nm, suggesting that **pyrene-PCBM** moieties attached to both sides of a single layer of the graphene sheet (see configuration (II), Scheme 2), thus, prohibiting the exfoliated single-layer graphene sheets from restacking.

Combining with the above Raman, SEM and AFM results, the geometric configuration of **rGO-pyrene-PCBM** can be elucidated as conformation (II) in Scheme 2, in which the C_{60} moiety is far from the graphene sheet and is bridged with the graphene sheet *via* the pyrene anchor.

Effect of rGO-pyrene-PCBM on the Performance of P3HT:PCBM BHJ-PSC Devices. As mentioned above, in previous reports, the applications of graphene in BHJ-PSCs were primarily focused on using graphenes as transparent electrode or electron acceptor materials.[8,11−14,17] In few reports, GO and rGO were also applied as interface layer materials, which typically function as hole transport layer, whereas the application of GO or rGO as electron extraction layer materials for improving the efficiency of negative charge collection and extraction was very limited.[8,12,18] Thus, considering the change transfer from **pyrene-PCBM** to rGO deduced from the Raman study above, we applied **rGO-pyrene-PCBM** as electron extraction layer for the most commonly studied P3HT:PCBM BHJ-PSCs and the device structure with **rGO-pyrene-PCBM** composite incorporated is shown in Scheme 3(I). The current density−voltage (J−V) curve of ITO/PEDOT:PSS/P3HT:PCBM/**rGO-pyrene-PCBM**/Al BHJ-PSC device fabricated at the optimized spin-coating speed is illustrated in Figure 7, which includes also those of using the component rGO or **pyrene-PCBM** as electron extraction layer for comparison. The measured parameters (open-circuit voltage (V_{oc}), short-circuit current (J_{sc}), fill factor (FF), PCE) are summarized in Table 1. The reference P3HT:PCBM BHJ-PSC device without any electron extraction layer (ITO/PEDOT:PSS/P3HT:PCBM/Al, device **A**) exhibited a PCE of 3.39%, which is comparable to the reported values with devices fabricated under similar conditions (chlorobenzene as solvent).[15,50−54] When **rGO-pyrene-PCBM** was incorporated as an electron extraction layer between the P3HT:PCBM photoactive layer and Al cathode, the PCE of the **rGO-pyrene-PCBM** incorporated device (device **B**) increases to 3.89%, which has a *ca.* 15% enhancement compared to that of reference P3HT:PCBM device. Contrarily, when **rGO-pyrene-PCBM** was substituted by its component rGO (device **C**) or **pyrene-PCBM** (device **D**), the obtained PCEs of the corresponding devices are 2.53% and 2.18%, respectively, which are both much lower than that of the reference P3HT:PCBM device (see Table 1). Given that the thicknesses of the **rGO-pyrene-PCBM**, rGO and **pyrene-PCBM** electron extraction layers (7−9 nm as determined by a surface profilometer, see Supporting Information S3) are quite comparable resulting from the identical spin-coating conditions, these results indicate clearly that only **rGO-pyrene-PCBM** composite performs as an efficient electron extraction

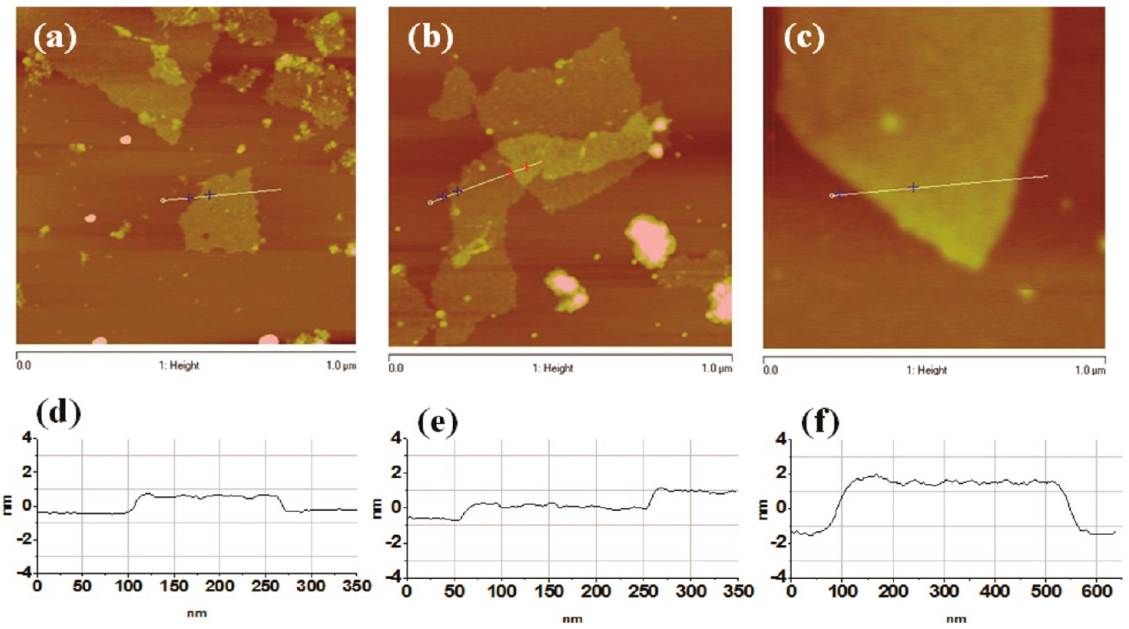

Figure 6. AFM images and the section analysis of GO (a and d), rGO (b and e) and rGO-pyrene-PCBM (c and f).

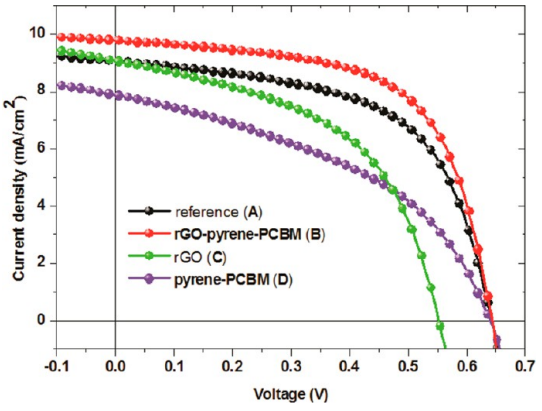

Figure 7. $J-V$ curves of the P3HT:PCBM BHJ-PSCs without (A) and with different electron extraction layers of rGO-pyrene-PCBM (B), rGO (C), and pyrene-PCBM (D). The devices were thermally annealed and the measurements were carried out under AM 1.5 illumination at an irradiation intensity of 100 mW·cm^{-2}.

layer whereas its components rGO or **pyrene-PCBM** could not play the same role independently, thus, unveiling the importance of composite formation between rGO and **pyrene-PCBM** components for its electron extraction property.

Figure 8 compares each photovoltaic parameter including V_{oc}, J_{sc}, and FF, and the factor(s) accounting for the change of PCE with the incorporation of different electron extraction layer could be analyzed. Compared to the reference P3HT:PCBM device (**A**), clearly the enhancement of PCE of the **rGO-pyrene-PCBM** incorporated device (**B**) originates from the increase of both J_{sc} (by *ca.* 9%) and FF (by *ca.* 6%), while V_{oc} keeps constant. When the pristine rGO was used as electron extraction layer (device **C**), J_{sc} exhibits a slight change ($\sim +2\%$), whereas both V_{oc} and FF

TABLE 1. Device Performances of P3HT:PCBM BHJ-PSCs with and without Electron Extraction Layers after Thermal Annealing

	electron extraction layer	V_{oc} (V)	J_{sc} (mA/cm^2)	FF (%)	PCE (%)	ΔPCE[a]
Device **A**	w/o	0.64	9.05	58.4	3.39	--
Device **B**	**rGO-pyrene-PCBM**	0.64	9.78	62.0	3.89	15%
Device **C**	rGO	0.55	9.07	50.7	2.53	−25%
Device **D**	**pyrene-PCBM**	0.64	7.86	43.5	2.18	−36%

[a] ΔPCE is the enhancement of PCE relative to the reference P3HT:PCBM BHJ-PSCs.

decrease dramatically, leading to an overall decrease of PCE by *ca.* 25%. Upon the incorporation of **pyrene-PCBM** (device **D**), both J_{sc} and FF decrease, resulting in the dramatic decrease of PCE by up to 36% (see Table 1 and Figure 8). Since V_{oc} is primarily correlated to the difference between the donor HOMO level and acceptor LUMO level,[55,56] the decrease in V_{oc} for the case of rGO incorporation should be due to the mismatching of their energy level with that of LUMO level of PCBM acceptor and Al cathode. Note that the drop in V_{oc} is found only when the pristine rGO was used as electron extraction layer, indicating that the pristine rGO is not a suitable electron extraction material for BHJ-PSC and this explains the reason why it was mainly used as hole transport material in previous reports.[8,16,57]

Among the determinative parameters of PCE, it is well-known that J_{sc} is dependent on not only the multiplication of the photo-induced charge carrier density and the charge carrier mobility within the active material, but also the interface properties between the active layers and the electrodes, while FF is determined by charge carriers reaching the electrodes when the built-in field is lowered toward the open circuit voltage.[58] Thus, the concurrent increase of both

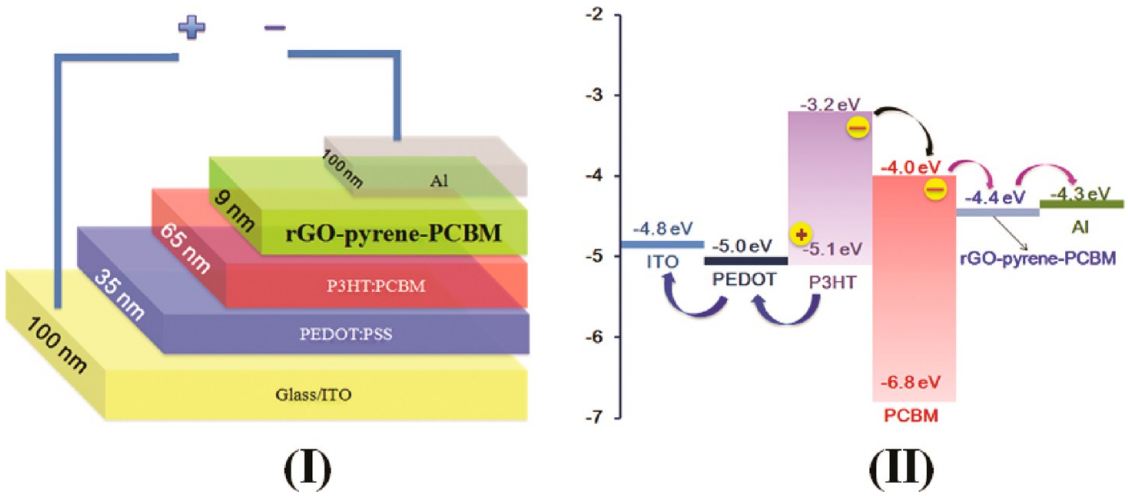

Scheme 3. The schematic architecture (I) and energy level diagram (II) of ITO/PEDOT:PSS/P3HT:PCBM/rGO-pyrene-PCBM/Al BHJ-PSC device with the incorporation of rGO-pyrene-PCBM electron extraction layer. The thickness of each layer was given in the left panel

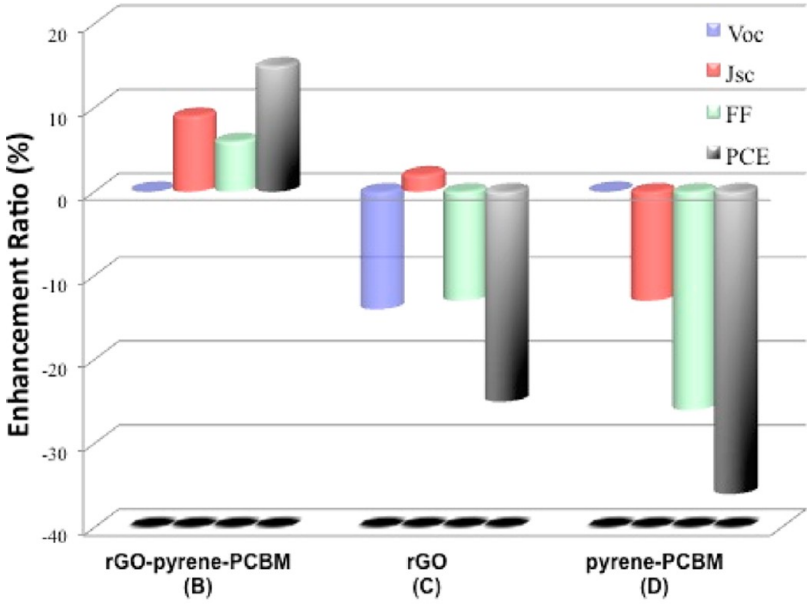

Figure 8. Enhancement ratio of the photovoltaic parameters of P3HT:PCBM BHJ-PSCs with different electron extraction layers of rGO-pyrene-PCBM, rGO, and pyrene-PCBM.

J_{sc} and FF observed for the **rGO-pyrene-PCBM** incorporated device is believed to result from the improvement of the P3HT:PCBM photoactive layer/Al electrode interface, for which it is known that there is a significant energy level offset (0.3 eV) between the work function of Al (4.3 eV) and the LUMO level of the PCBM acceptor (4.0 eV) resulting in the unfavorable electron extraction (see Scheme 3(II)).[51−53,59] To facilitate the electron extraction from the active layer to the cathode electrode, preferably the work function of the cathode should be aligned with the LUMO level of the acceptor so as to form Ohmic contact. Contrary to rGO which has the mismatching on energy level with that of the LUMO level of PCBM acceptor and Al cathode as revealed by the decrease of V_{oc}, the attachment of **pyrene-PCBM** onto rGO within the **rGO-pyrene-PCBM** composite leads to the charge transfer from **pyrene-PCBM** to rGO as deduced from the Raman study above, and as a result, the work function of **rGO-pyrene-PCBM** composite has presumably a better matching with the LUMO level of PCBM acceptor, and the **rGO-pyrene-PCBM** modified Al cathode can form an Ohmic contact with the P3HT:PCBM active layer for efficient electron extraction.[60,61] A similar interpretation was proposed by Dai *et al.* for the first application of a cesium-neutralized GO (GO-Cs) as an efficient electron extraction layer for both normal and inverted P3HT:PCBM BHJ-PSCs.[18] Such an assumption was experimentally confirmed by the estimation of work functions of different electron extraction materials which

were calculated from the surface potentials measured by Scanning Kelvin probe microscopy (SKPM).[62,63] Taking −4.5 eV as the work function of HOPG used as reference,[62,63] the work functions of **rGO-pyrene-PCBM**, rGO, and **pyrene-PCBM** are estimated to be −4.4, −4.6, and −4.2 eV, respectively (see Supporting Information S4). Clearly, the work function of **rGO-pyrene-PCBM** (−4.4 eV), which is between the rGO and **pyrene-PCBM** components, shows the best matching with that of P3HT:PCBM reference (see Scheme 3(II)), thus, leading to the obvious enhancement of PCE. Contrarily, since the work function of rGO is too high (−4.6 eV), its incorporation as electron extraction layer resulted in the much lower V_{oc} (0.55 V) and consequently lowered PCE. For the case of using **pyrene-PCBM** as electron extraction layer, although its work function (−4.2 eV) has a reasonable matching with that of P3HT:PCBM reference as well, the strong electron-donating ability of the pyrene moiety might prohibit the electron extraction as suggested by the decrease of both J_{sc} and FF (see Table 1).

It should be noted that, since **rGO-pyrene-PCBM** represents the first graphene−PCBM composite, another intuitive idea is to use **rGO-pyrene-PCBM** in the active layer in the way of either substituting PCBM or doping in P3HT:PCBM layer. Because the low solubility of rGO in those organic solvents such as chlorobenzene and chloroform, which are commonly used to dissolve P3HT and PCBM active layer materials used in the state-of-art BHJ-PSCs,[64] is largely preserved in **rGO-pyrene-PCBM** composite, it seems quite difficult to completely substitute PCBM with **rGO-pyrene-PCBM** as the new acceptor material due to the demand of the relatively high concentration of the active layer solution for fabricating film by spin-coating. Therefore, alternatively, **rGO-pyrene-PCBM** composite was dispersed in chlorobenzene and doped into the P3HT:PCBM active layer with a relatively low doping ratio (∼1 wt %), and the PCE of the device doped by **rGO-pyrene-PCBM** is quite comparable to that of reference without doping (see Supporting Information Figure S4 and Table S3 for the comparison of the *J*−*V* curve and photovoltaic parameters). Doping **rGO-pyrene-PCBM** composite into P3HT:PCBM active layer with a ratio higher than 1 wt % led to inhomogeous active layer film because the aggregation size of **rGO-pyrene-PCBM** composite dispersed in chlorobenzene was too large upon overdoping. These results indicate that **rGO-pyrene-PCBM** doped in the P3HT:PCBM active layer has little influence on the performance of BHJ-PSCs presumably owing to the relatively low doping ratio, thus, confirming that **rGO-pyrene-PCBM** preferably functions as an efficient electron extraction material in BHJ-PSCs.

CONCLUSION

In summary, for the first time, PCBM as the most commonly used acceptor material in BHJ-PSCs was attached onto rGO *via* the noncovalent functionalization approach with pyrene used as an anchoring bridge, affording a new graphene−fullerene composite **rGO-pyrene-PCBM**. The hybrid structure of **rGO-pyrene-PCBM** was confirmed by various spectroscopic characterizations including FTIR, UV−vis, and XPS. Compared to the pristine rGO, the dispersity of **rGO-pyrene-PCBM** in DMF was greatly improved because of the intramolecular $\pi-\pi$ stacking interactions between the graphene sheet and **pyrene-PCBM**. On the basis of Raman, SEM, and AFM studies, the geometric configuration of **rGO-pyrene-PCBM** was proposed where the C_{60} moiety is far from the graphene sheet and is bridged with the graphene sheet *via* the pyrene anchor. Raman study suggested further that a charge transfer from **pyrene-PCBM** to rGO takes place for **rGO-pyrene-PCBM**. Finally, **rGO-pyrene-PCBM** was successfully applied as an electron extraction material for P3HT:PCBM BHJ-PSC devices, leading to the efficiency enhancement by *c*a. 15%, whereas using the rGO or **pyrene-PCBM** component as electron extraction layer resulted in dramatic decrease of PCE instead. These results reveal the importance of composite formation between rGO and **pyrene-PCBM** components for its electron extraction property. As the first graphene−PCBM composite with excellent electron extraction property, this study paves the way for constructing new graphene-based composite toward the application in polymer solar cells.

EXPERIMENTAL SECTION

Materials. Poly (3-hexylthiophene) (P3HT) and (6,6)-phenyl-C61-butyric acid methyl ester (PCBM) were bought from Luminescence Technology Corp. and Nichem Fine Technology Co., Ltd., respectively. 1-Pyrene butanol, 4-(dimethylamino) pyridine (DMAP), and nano graphite powder were purchased from Aldrich, Alfa Aesar, and Aladdin, respectively. The glacial acetic acid, concentrated sulfuric acid, concentrated hydrochloric acid (30%), *N*,*N*′-dicyclohexylcarbodiimide (DCC), sodium methylate, $K_2S_2O_8$, $KMnO_4$, P_2O_5, H_2O_2, aqueous ammonia, and hydrazine hydrate were purchased from Sinopharm Chemical Reagent Co. Ltd., China. Poly (3,4-ethylenedioxythiophene):polystyrene sulfonic acid (PEDOT:PSS, Baytron P) was purchased from SCM Industrial Chemical Co., Ltd. All the reagents were directly used as received without further purification unless specially mentioned.

Characterization. ^{1}H NMR spectra were recorded on a Bruker AV400 NMR instrument using tetramethylsilane (TMS) as an internal reference. FTIR spectra were recorded on a TENSOR 27 spectrometer (Bruker, Germany) at room temperature by dropping samples onto KBr pellet. UV−vis absorption spectra were measured on a UV-3600 spectrometer (Shimadzu, Japan) using a quartz cell of 10 mm layer thickness and 1 nm resolution. Raman spectra were taken at room temperature with a LABRAM-HR equipment (Jobin Yvon, France) operating at a wavelength of 514.5 nm as the excitation source, and the samples were dropped onto silicon substrates and dried into a film. X-ray photoelectron spectroscopy (XPS) was conducted on an

ESCALAB 250 (Thermo-VV Scientific) instrument. A JEOL JSM-7401F instrument (Japan) was used for SEM imaging. The atomic force microscopy (AFM) images were taken using a Nanoscope III (Digital Instruments) operating in height mode by dropping samples on new cleaved mica and dried in atmosphere. Scanning Kelvin probe microscopy (SKPM) measurements were carried out on AFM using the standard SKPM mode. A surface profilometer (KLA-Tencor P6) was used to measure the film thickness.

Synthesis. The synthetic route of the new graphene–fullerene composite (**rGO-pyrene-PCBM**) is shown in Scheme 1. The detailed synthetic procedures are as follow:

Synthesis of [6,6]-Phenyl-C61-butyric Acid 1-Pyrene Butyl Ester (Pyrene-PCBM). [6, 6]-Phenyl-C61-butyric acid (PCBA) as the carboxylated PCBM was synthesized according to the literature method.[33−35] Briefly, PCBM (75 mg, 0.082 mmol) was dissolved in 100 mL of toluene (0.82 mmol·L^{-1}) under heating at 110 °C with stirring for 2 h, then glacial CH_3COOH (50 mL) and diluted HCl (20 mL) were added. The mixture was stirred and refluxed for 12 h, and the reaction was monitored by TLC (silica/toluene). All the volatile components were then removed in vacuum and the residue was transferred into a glass centrifuge bottle and treated with methanol and toluene to precipitate the product. The residue was dried in vacuum at 60 °C, affording 50 mg of PCBA. PCBA (50 mg, 0.056 mmol) was redissolved in a mixture solvent of CS_2 and CH_2Cl_2 (1:1 v/v). 1-Pyrene butanol (62 mg, 0.23 mmol) was added then into the mixture, and ultrasonicated for 3 min to achieve a homogeneous solution. The mixture was stirred at room temperature with N_2 protection for 30 min. Then *N,N′*-dicyclohexylcarbodiimide (DCC) (14 mg, 0.068 mmol) and dimethylamino pyridine (DMAP) (2.7 mg, 0.022 mmol) dissolved in 3 mL of CH_2Cl_2 were added into the mixture, stirring for 3 days. During the reaction, the mixture turned clear and then orchid color. After the reaction, the mixture was concentrated to 5 mL through N_2 blowing, then centrifuged at 9000 rpm for 3 min to precipitate the unreacted PCBA and DCC hydrate produced during the reaction. The resultant mixture was purified by column chromatography (CC): SiO_2 (100−200 and 200−300 mesh) and dried under vacuum (27.5 mg). ^{1}H NMR (300 MHz, $CDCl_3$) δ (ppm): 8.25 (dd, J = 9.3, 3.7 Hz, 1H), 8.18−8.07 (m, 4H), 8.03−7.94 (m, 3H), 7.88−7.80 (m, 3H), 7.51−7.37 (m, 3H), 4.15 (t, J = 6.3 Hz, 2H), 3.38 (dd, J = 14.9, 7.5 Hz, 2H), 2.93−2.79 (m, 2H), 2.51 (t, J = 7.2 Hz, 2H), 2.22−2.08 (m, 2H), 1.99−1.87 (m, 2H), 1.81 (dt, J = 11.9, 6.3 Hz, 2H).

Preparation of Chemically Reduced Graphene Oxide (rGO) and Graphene–Fullerene Composite (rGO-Pyrene-PCBM). GO was synthesized from nano graphite powder by a modified Hummers method.[39] Chemically reduced graphene oxide (rGO) was prepared through the modified method reported by Li and co-workers.[40] Briefly, the as-prepared homogeneous *N,N*-dimethylformamide (DMF) dispersion of GO (2.0 mL, 1.6 mg/mL) was mixed with 14.0 mL of DMF, 50 μL of hydrazine solution (85 wt % in water), and aqueous ammonia (28 wt % in water, the amount of ammonia solution was monitored by pH = 10) in a three-necked bottle. After vigorously shaking or stirring for a few minutes, the three-necked bottle was placed in an oil bath (~95 °C) for 1 h. After reduction, a homogeneous black dispersion with a small amount of black precipitate was obtained. The resultant mixture solution was centrifuged at 9000 rpm for 15 min to remove any visible precipitate. The reserved liquid was further centrifuged at 9000 rpm for 10 min, and a stable, homogeneous black dispersion of rGO without any precipitate was obtained. To prepare for the dispersion of graphene–fullerene composite (**rGO-pyrene-PCBM**), 2 mL of **pyrene-PCBM** solution in DMF (1.6 mg/mL, 1.39 × 10^{-3} mmol·L^{-1}) was added into the GO dispersion before the additions of hydrazine and ammonia, followed by the reduction procedure described above. A homogeneous dispersion of **rGO-pyrene-PCBM** without any macroscopic precipitate was achieved and a further centrifugation at 9000 rpm could not yield any precipitate either. Washing the dispersion of **rGO-pyrene-PCBM** by toluene and CS_2 did not generate any dissolved fullerene moiety.

BHJ-PSC Device Fabrication and Measurements. Our detailed fabrication procedure of the P3HT:PCBM BHJ-PSC devices has been reported previously.[34,50−53] Briefly, the ITO-coated glass substrate (8Ω/□, purchased from Shenzhen Nan Bo Group, China) was first cleaned with detergent, then ultrasonicated in acetone and 2-propanol, and subsequently dried in vacuum at 60 °C overnight. PEDOT:PSS (Baytron P) layer (~35 nm thick) was spin-coated onto the ITO substrate and then annealed at 120 °C for 30 min. The P3HT:PCBM (1:0.8 w/w) blend was dissolved in chlorobenzene by stirring at 40 °C until all the materials dissolved, which was spin-coated onto the PEDOT:PSS layer affording the P3HT:PCBM active layer (~ 65 nm thick). To prepare for the device with **rGO-pyrene-PCBM** incorporated as electron extraction layer, **rGO-pyrene-PCBM** was dispersed in the mixture solution of DMF and 2-propanol with a concentration of ~0.35 mg/mL, and then spin-coated onto the P3HT:PCBM active layer at 3000 rpm for 60 s. All of the solution processing and film preparation were carried out in air atmosphere. The device was then transferred into vacuum chamber (~10^{-5} Torr), and an Al electrode (~ 100 nm thick) was deposited on the top of the active layer through a shadow mask to define the active area of the devices (2 × 5 mm^2). Finally, thermal annealing was carried out at 150 °C for 10 min on a digital hot plate under a nitrogen atmosphere inside a glovebox.

PCE was measured under simulated AM 1.5 irradiation (100 mW cm^{-2}) using a standard xenon-lamp-based solar simulator (Oriel Sol 3A), for which the illumination intensity was calibrated by a monocrystalline silicon reference cell (Oriel P/N 91150 V, with KG-5 visible color filter) calibrated by the National Renewable Energy Laboratory (NREL). The current–voltage (J–V) characteristics were measured with a Keithley 2400 source meter. All the measurements were carried out in air atmosphere and a mask with well-defined area size of 10.0 mm^2 was attached onto the cell to define the effective area so as to ensure the accurate measurement. More than 10 devices were fabricated independently under each experimental condition and measured to ensure the consistency of the data, and the average results were used in the following discussions.

Conflict of Interest: The authors declare no competing financial interest.

Acknowledgment. This work was partially supported by National Basic Research Program of China (2010CB923300, 2011CB921400), National Natural Science Foundation of China (Nos. 90921013, 21132007), "100 Talents Programme of CAS" from Chinese Academy of Sciences, the Fundamental Research Funds for the Central Universities (WK2060140005), Key Laboratory of Novel Thin Film Solar Cells (KF201103), Chinese Academy of Sciences, and Specialized Research Fund for the Doctoral Program of Higher Education (No. 20113402110020).

Supporting Information Available: ^{1}H NMR spectra of **rGO-py-PCBM** and PCBA, close-up analysis of the binding energy (BE) of C_{1s} core, measurements of the thickness of electron extraction layer, determination of work function by SKPM, J–V curve and photovoltaic parameters of devices with **rGO-pyrene-PCBM** composite doped in P3HT:PCBM active layer, *etc.* This material is available free of charge *via* the Internet at http://pubs.acs.org.

REFERENCES AND NOTES

1. Geim, A. K.; Novoselov, K. S. The Rise of Graphene. *Nat. Mater.* **2004**, *6*, 183–191.
2. Novoselov, K. S.; Geim, A. K.; Morozov, S. V.; Jiang, D.; Zhang, Y.; Dubonos, S. V.; Grigorieva, I. V.; Firsov, A. A. Electric Field Effect in Atomically Thin Carbon Films. *Science* **2004**, *306*, 666–669.
3. Zhang, Y.; Tan, Y. W.; Stormer, H. L.; Kim, P. Experimental Observation of the Quantum Hall Effect and Berry's Phase in Graphene. *Nature* **2005**, *438*, 201–204.
4. Nair, R. R.; Blake, P.; Grigorenko, A. N.; Novoselov, K. S.; Booth, T. J.; Stauber, T.; Peres, N. M. R.; Geim, A. K. Fine Structure Constant Defines Visual Transparency of Graphene. *Science* **2008**, *320*, 1308.
5. Zhu, Y. W.; Murali, S.; Stoller, M. D.; Ganesh, K. J.; Cai, W. W.; Ferreira, P. J.; Pirkle, A.; Wallace, R. M.; Cychosz, K. A.; Thommes, M.; Su, D.; *et al.* Carbon-Based Supercapacitors Produced by Activation of Graphene. *Science* **2011**, *332*, 1537–1541.

6. Lee, C.; Wei, X.; Kysar, J. W.; Hone, J. Measurement of the Elastic Properties and Intrinsic Strength of Monolayer Graphene. *Science* **2008**, *321*, 385–388.
7. Balandin, A. A.; Ghosh, S.; Bao, W.; Calizo, I.; Teweldebrhan, D.; Miao, F.; Lau, C. N. Superior Thermal Conductivity of Single-Layer Graphene. *Nano Lett.* **2008**, *8*, 902–907.
8. Wan, X.; Long, G.; Huang, L.; Chen, Y. Graphene—A Promising Material for Organic Photovoltaic Cells. *Adv. Mater.* **2011**, *23*, 5342–5358.
9. Guo, C. X.; Guai, G. H.; Li, C. M. Graphene Based Materials: Enhancing Solar Energy Harvesting. *Adv. Energy Mater.* **2011**, *1*, 448–452.
10. Meric, I.; Han, M. Y.; Young, A. F.; Ozyilmaz, B.; Kim, P.; Shepard, K. L. Current Saturation in Zero-Bandgap, Top-Gated Graphene Field-Effect Transistors. *Nat. Nanotechnol.* **2008**, *3*, 654–659.
11. Wan, X.; Hang, Y.; Chen, Y. Focusing on Energy and Optoelectronic Applications: A Journey for Graphene and Graphene Oxide at Large Scale. *Acc. Chem. Res.* **2011**, *45*, 598–607.
12. Dai, L. Functionalization of Graphene for Efficient Energy Conversion and Storage. *Acc. Chem. Res.* **2013**, *46*, 31–42.
13. Huang, X.; Zeng, Z.; Fan, Z.; Liu, J.; Zhang, H. Graphene-Based Electrodes. *Adv. Mater.* **2012**, *24*, 5979–6004.
14. Pang, S.; Hernandez, Y.; Feng, X.; Mullen, K. Graphene as Transparent Electrode Material for Organic Electronics. *Adv. Mater.* **2011**, *23*, 2779–2795.
15. Wang, Y.; Tong, S. W.; Xu, X. F.; Ozyilmaz, B.; Loh, K. P. Interface Engineering of Layer-by-Layer Stacked Graphene Anodes for High-Performance Organic Solar Cells. *Adv. Mater.* **2011**, *23*, 1514–1518.
16. Li, S.-S.; Tu, K.-H.; Lin, C.-C.; Chen, C.-W.; Chhowalla, M. Solution-Processable Graphene Oxide as an Efficient Hole Transport Layer in Polymer Solar Cells. *ACS Nano* **2010**, *4*, 3169–3174.
17. Liu, Z.; He, D.; Wang, Y.; Wu, H.; Wang, J. Solution-Processable Functionalized Graphene in Donor/Acceptor-Type Organic Photovoltaic Cells. *Sol. Energy Mater. Sol. Cells* **2010**, *94*, 1196–1200.
18. Liu, J.; Xue, Y.; Gao, Y.; Yu, D.; Durstock, M.; Dai, L. Hole and Electron Extraction Layers Based on Graphene Oxide Derivatives for High-Performance Bulk Heterojunction Solar Cells. *Adv. Mater.* **2012**, *24*, 2228–2233.
19. Huang, X.; Qi, X.; Boey, F.; Zhang, H. Graphene-Based Composites. *Chem. Soc. Rev.* **2012**, *41*, 666–686.
20. Ahmad, I.; Khan, U.; Gun'ko, Y. K. Graphene, Carbon Nanotube and Ionic Liquid Mixtures: Towards New Quasi-Solid State Electrolytes for Dye Sensitised Solar Cells. *J. Mater. Chem* **2011**, *21*, 16990–16996.
21. Stankovich, S.; Dikin, D. A.; Dommett, G. H.; Kohlhaas, K. M.; Zimney, E. J.; Stach, E. A.; Piner, R. D.; Nguyen, S. T.; Ruoff, R. S. Graphene-Based Composite Materials. *Nature* **2006**, *442*, 282–286.
22. Lu, T.; Zhang, Y.; Li, H.; Pan, L.; Li, Y.; Sun, Z. Electrochemical Behaviors of Graphene−ZnO and Graphene−SnO_2 Composite Films for Supercapacitors. *Electrochim. Acta* **2010**, *55*, 4170–4173.
23. Su, Q.; Pang, S.; Alijani, V.; Li, C.; Feng, X.; Müllen, K. Composites of Graphene with Large Aromatic Molecules. *Adv. Mater.* **2009**, *21*, 3191–3195.
24. Tung, V. C.; Huang, J. H.; Tevis, I.; Kim, F.; Kim, J.; Chu, C. W.; Stupp, S. I.; Huang, J. X. Surfactant-Free Water-Processable Photoconductive All-Carbon Composite. *J. Am. Chem. Soc.* **2011**, *133*, 4940–4947.
25. Zhang, X.; Huang, Y.; Wang, Y.; Ma, Y.; Liu, Z.; Chen, Y. Synthesis and Characterization of a Graphene−C60 Hybrid Material. *Carbon* **2009**, *47*, 334–337.
26. Zhang, Y.; Ren, L.; Wang, S.; Marathe, A.; Chaudhuri, J.; Li, G. Functionalization of Graphene Sheets through Fullerene Attachment. *J. Mater. Chem* **2011**, *21*, 5386–5398.
27. Zhang, X.; Liu, Z.; Huang, Y.; Wan, X.; Tian, J.; Ma, Y.; Chen, Y. Synthesis, Characterization and Nonlinear Optical Property of Graphene-C60 Hybrid. *J. Nanosci. Nanotechnol.* **2009**, *9*, 5752–5756.
28. Tung, V. C.; Huang, J. H.; Kim, J.; Smith, A. J.; Chu, C. W.; Huang, J. X. Towards Solution Processed All-Carbon Solar Cells: A Perspective. *Energy Environ. Sci.* **2012**, *5*, 7810–7818.
29. Ramuz, M. P.; Vosgueritchian, M.; Wei, P.; Wang, C.; Gao, Y.; Wu, Y.; Chen, Y.; Bao, Z. Evaluation of Solution-Processable Carbon-Based Electrodes for All-Carbon Solar Cells. *ACS Nano* **2012**, *6*, 10384–10395.
30. Lohrman, J.; Kumar, P. V.; Kirkeminde, A.; Ferralis, N.; Grossman, J. C.; Ren, S. Nanocarbon-Based Photovoltaics. *ACS Nano* **2012**, *6*, 8896–8903.
31. Liu, Z. B.; Xu, Y. F.; Zhang, X. Y.; Zhang, X. L.; Chen, Y. S.; Tian, J. G. Porphyrin and Fullerene Covalently Functionalized Graphene Hybrid Materials with Large Nonlinear Optical Properties. *J. Phys. Chem. B* **2009**, *113*, 9681–9686.
32. Yu, D.; Park, K.; Durstock, M.; Dai, L. Fullerene-Grafted Graphene for Efficient Bulk Heterojunction Polymer Photovoltaic Devices. *J. Phys.Chem. Lett.* **2011**, *2*, 1113–1118.
33. Hummelen, J. C.; Knight, B. W.; LePeq, F.; Wudl, F.; Yao, J.; Wilkins, C. L. Preparation and Characterization of Fulleroid and Methanofullerene Derivatives. *J. Org. Chem.* **1995**, *60*, 532–538.
34. Chen, M.; Li, M.; Wang, H.; Qu, S.; Zhao, X.; Xie, L.; Yang, S. Side-Chain Substitution of Poly(3-hexylthiophene) (P3HT) by PCBM *via* Postpolymerization: An Intramolecular Hybrid Of Donor and Acceptor. *Polym. Chem.* **2013**, *4*, 550–557.
35. Chen, L.; Yao, K.; Chen, Y. Can Morphology Tailoring Based on Functionalized Fullerene Nanostructures Improve the Performance of Organic Solar Cells? *J. Mater. Chem.* **2012**, *22*, 18768–18771.
36. Neises, B.; Steglich, W. Simple Method for the Esterification of Carboxylic Acids. *Angew. Chem., Int. Ed. Engl.* **1978**, *17*, 522–524.
37. Xu, Y.; Bai, H.; Lu, G.; Li, C.; Shi, G. Flexible Graphene Films *via* the Filtration of Water-Soluble Noncovalent Functionalized Graphene Sheets. *J. Am. Chem. Soc.* **2008**, *130*, 5856–5857.
38. Li, M.; Xu, P.; Yang, J.; Ying, H.; Haubner, K.; Dunsch, L.; Yang, S. Synthesis of Pyrene-Substituted Poly(3-hexylthiophene) *via* Postpolymerization and Its Noncovalent Interactions with Single-Walled Carbon Nanotubes. *J. Phys. Chem. C* **2011**, *115*, 4584–4593.
39. Hummers, W. S., Jr.; Offeman, R. E. Preparation of Graphitic Oxide. *J. Am. Chem. Soc.* **1958**, *80*, 1339–1339.
40. Li, D.; Muller, M. B.; Gilje, S.; Kaner, R. B.; Wallace, G. G. Processable Aqueous Dispersions of Graphene Nanosheets. *Nat. Nanotechnol.* **2008**, *3*, 101–105.
41. Chen, J. L.; Yan, X. P. A Dehydration and Stabilizer-Free Approach to Production of Stable Water Dispersions of Graphene Nanosheets. *J. Mater. Chem.* **2010**, *20*, 4328–4332.
42. Szabó, T.; Berkesi, O.; Forgó, P.; Josepovits, K.; Sanakis, Y.; Petridis, D.; Dékány, I. Evolution of Surface Functional Groups in a Series of Progressively Oxidized Graphite Oxides. *Chem. Mater.* **2006**, *18*, 2740–2749.
43. Chiang, T. C.; Seitz, F. Photoemission Spectroscopy in Solids. *Ann. Phys.* **2001**, *10*, 61–74.
44. Yang, D.; Velamakanni, A.; Bozoklu, G.; Park, S.; Stoller, M.; Piner, R. D.; Stankovich, S.; Jung, I.; Field, D. A.; Ventrice, C. A.; *et al.* Chemical Analysis of Graphene Oxide Films after Heat and Chemical Treatments by X-ray Photoelectron and Micro-Raman Spectroscopy. *Carbon* **2009**, *47*, 145–152.
45. Kang, H.; Kulkarni, A.; Stankovich, S.; Ruoff, R. S.; Baik, S. Restoring Electrical Conductivity of Dielectrophoretically Assembled Graphite Oxide Sheets by Thermal and Chemical Reduction Techniques. *Carbon* **2009**, *47*, 1520–1525.
46. Ferrari, A. C.; Meyer, J. C.; Scardaci, V.; Casiraghi, C.; Lazzeri, M.; Mauri, F.; Piscanec, S.; Jiang, D.; Novoselov, K. S.; Roth, S.; *et al.* Raman Spectrum of Graphene and Graphene Layers. *Phys. Rev. Lett.* **2006**, *97*, 187401.
47. Ferrari, A. C.; Robertson, J. Interpretation of Raman Spectra of Disordered and Amorphous Carbon. *Phys. Rev. B* **2000**, *61*, 14095–14107.
48. Parviz, D.; Das, S.; Ahmed, H. S. T.; Irin, F.; Bhattacharia, S.; Green, M. J. Dispersions of Non-Covalently Functionalized Graphene with Minimal Stabilizer. *ACS Nano* **2012**, *6*, 8857–8867.

49. Gómez-Navarro, C.; Weitz, R. T.; Bittner, A. M.; Scolari, M.; Mews, A.; Burghard, M.; Kern, K. Electronic Transport Properties of Individual Chemically Reduced Graphene Oxide Sheets. *Nano Lett.* **2007**, *7*, 3499–3503.
50. Zhang, W.; Xu, Y.; Wang, H.; Xu, C.; Yang, S. Fe_3O_4 Nanoparticles Induced Magnetic Field Effect on Efficiency Enhancement of P3HT:PCBM Bulk Heterojunction Polymer Solar Cells. *Sol. Energy Mater. Sol. Cells* **2011**, *95*, 2880–2885.
51. Zhang, W.; Wang, H.; Chen, B.; Bi, X.; Venkatesan, S.; Qiao, Q.; Yang, S. Oleamide as a Self-Assembled Cathode Buffer Layer for Polymer Solar Cells: The Role of the Terminal Group on the Function of the Surfactant. *J. Mater. Chem* **2012**, *22*, 24067.
52. Wang, H.; Zhang, W.; Xu, C.; Bi, X.; Chen, B.; Yang, S. Efficiency Enhancement of Polymer Solar Cells by Applying Poly(vinylpyrrolidone) as Cathode Buffer Layer *via* Spin-Coating or Self-Assembly. *ACS Appl. Mater. Inerfaces* **2013**, *5*, 26–34.
53. Wang, H.; Zhang, W.; Chen, B.; Yang, S. Enhancing Power Conversion Eficiency of Polymer Solar Cels *via* Treatment of PEDOT:PSS Anode Bufer Layer Using DMF Solvent. *J. Univ. Sci. Technol. China* **2012**, *42*, 775–784.
54. Dang, M. T.; Hirsch, L.; Wantz, G. P3HT:PCBM, Best Seller in Polymer Photovoltaic Research. *Adv. Mater.* **2011**, *23*, 3597–3602.
55. Rauh, D.; Wagenpfahl, A.; Deibel, C.; Dyakonov, V. Relation of Open Circuit Voltage to Charge Carrier Density in Organic Bulk Heterojunction Solar Cells. *Appl. Phys. Lett.* **2011**, *98*, 133301.
56. Mihailetchi, V. D.; Blom, P. W. M.; Hummelen, J. C.; Rispens, M. T. Cathode Dependence of the Open-Circuit Voltage of Polymer:Fullerene Bulk Heterojunction Solar Cells. *J. Appl. Phys.* **2003**, *94*, 6849–6854.
57. Jeon, Y. J.; Yun, J. M.; Kim, D. Y.; Na, S. I.; Kim, S. S. High-Performance Polymer Solar Cells with Moderately Reduced Graphene Oxide as an Efficient Hole Transporting Layer. *Sol. Energy Mater. Sol. Cells* **2012**, *105*, 96–102.
58. Gunes, S.; Neugebauer, H.; Sariciftci, N. S. Conjugated Polymer-Based Organic Solar Cells. *Chem. Rev.* **2007**, *107*, 1324–1338.
59. Chen, L. M.; Xu, Z.; Hong, Z. R.; Yang, Y. Interface Investigation and Engineering—Achieving High Performance Polymer Photovoltaic Devices. *J. Mater. Chem.* **2010**, *20*, 2575–2598.
60. Po, R.; Carbonera, C.; Bernardi, A.; Camaioni, N. The Role of Buffer Layers in Polymer Solar Cells. *Energy Environ. Sci.* **2011**, *4*, 285–310.
61. Yip, H.-L.; Jen, A. K. Y. Recent Advances in Solution-Processed Interfacial Materials for Efficient and Stable Polymer Solar Cells. *Energy Environ. Sci.* **2012**, *5*, 5994–6011.
62. Palma, M.; Levin, J.; Lemaur, V.; Liscio, A.; Palermo, V.; Cornil, J.; Geerts, Y.; Lehmann, M.; Samorì, P. Self-Organization and Nanoscale Electronic Properties of Azatriphenylene-Based Architectures: A Scanning Probe Microscopy Study. *Adv. Mater.* **2006**, *18*, 3313–3317.
63. Wang, X.; Zhi, L.; Mullen, K. Transparent, Conductive Graphene Electrodes for Dye-Sensitized Solar Cells. *Nano Lett.* **2008**, *8*, 323–327.
64. Dang, M. T.; Wantz, G.; Bejbouji, H.; Urien, M.; Dautel, O. J.; Vignau, L.; Hirsch, L. Polymeric Solar Cells Based on P3HT: PCBM: Role of the Casting Solvent. *Sol. Energy Mater. Sol. Cells* **2011**, *95*, 3408–3418.